Journal of Applied Electrochemistry **32**: 487–496, 2002.

An electrochemical study of the behaviour of ear piercing studs immersed in a culture medium

J.M. BASTIDAS[1]*, M. SAIKI[2], S.O. ROGERO[2], I. COSTA[2] and J.L. POLO[3]
[1]*CENIM-National Centre for Metallurgical Research, CSIC, Avda. Gregorio del Amo 8, 28040 Madrid, Spain*
[2]*Instituto de Pesquisas Energéticas e Nucleares (IPEN/CNEN-SP), Caixa Postal 11049, Cidade Universitaria, CEP 05422-970 São Paulo, Brazil*
[3]*School of Industrial Engineering, University of Castilla-La Mancha, Avda. Carlos III s/n, 45071 Toledo, Spain*
*(*author for correspondence, fax: +34 91 534 7425, e-mail: bastidas@cenim.csic.es)*

Received 9 February 2001; accepted in revised form 5 March 2002

Key words: corrosion, cytotoxicity, ear piercing stud, electrochemical methods

Abstract

Two commercial studs, of gold-coated stainless steel and copper–zinc alloy, respectively, and a laboratory-made titanium stud were chosen for corrosion studies. Corrosion behaviour in a culture medium (CM) was studied using electrochemical impedance spectroscopy and polarization measurements, as a function of immersion time. The elements that leached out into the CM electrolyte were analysed by instrumental neutron activation analysis. Scanning electron microscopy and energy dispersive X-ray techniques were utilized in the analysis of the stud surfaces before and after their immersion in a CM solution. The cytotoxicity of the tested studs was also determined. The titanium stud showed the best combination of properties, high corrosion resistance and low cytotoxicity, while the gold-coated stainless steel stud occupied an intermediate position.

1. Introduction

Gold coatings are frequently applied on piercing stud surfaces for aesthetic reasons, corrosion resistance, and because gold has little or no cytotoxicity [1]. Gold coatings should be compact and adherent to the substrate to prevent contact between alloying elements in the substrate and body fluids while the pierced earlobes are healing. In practice the coating process introduces defects which allow corrosion of the substrate to take place, with the release of nickel ions. Nickel-containing alloys have been widely used as substrates in the manufacture of ear piercing studs. Skin sensitisation has been related to nickel ions, which can leach out into body fluids in corrosion reactions. Nickel ions are the main cause of allergic contact dermatitis [2–7], since they bind to tissue and interstitial fluid proteins [3]. The elements leached out during the corrosion of two alloys used for ear piercing studs have been determined using neutron activation analysis (NAA) in a previous paper [8].

This paper is a contribution to the study of the corrosion resistance of two commercial gold-coated alloys, one with a stainless steel substrate and the other with a copper–zinc based alloy substrate, that are being used in the manufacture of ear piercing studs. These alloys are also being linked to allergic reactions. A laboratory-made titanium stud was also tested as a potential material for ear piercing studs.

2. Materials and methods

Three types of ear piercing studs have been studied: (i) gold-coated austenitic stainless steel (GSS), (ii) gold-coated copper–zinc alloy (GCZ), and (iii) titanium (Ti).

Table 1 shows the chemical composition of uncoated substrates from ear piercing studs. NAA was utilized to analyse the stems and butterfly backs of the studs separately, after removing the gold coating [9].

Corrosion behaviour of the studs was investigated using electrochemical impedance spectroscopy (EIS) and DC polarization techniques. The EIS method was used in the frequency range from 50 kHz to 3.15 mHz, with a logarithmic sweeping frequency of 10 steps per decade. Impedance data was generated at the corrosion potential (E_{corr}). EIS involved the imposition of a 0.01 V amplitude sine wave. A Solartron 1250 frequency response analyser connected to an EG&G PARC 273A potentiostat was used. These measurements were carried out in a culture medium (CM), see Table 2, at room temperature (~25 °C). A three-electrode cell arrangement was used for the electrochemical EIS and DC tests, with a graphite rod as counter electrode, a

Table 1. Chemical composition of the uncoated substrate of ear piercing studs

Element	Stainless steel		Copper–zinc		Titanium	
	Concentration					
	/%	/ppm	/%	/ppm	/%	/ppm
As	–	54.7 ± 0.8	–	8.1 ± 0.5	–	17.7 ± 0.3
Co	–	2203 ± 11	–	27.4 ± 0.4	–	≤1
V	–	987 ± 26	–	≤77	–	33 ± 3
Cr	16.1	–	≤0.007	–	≤0.01	–
Cu	0.35	–	36.5	–	≤0.04	–
Fe	67.9	–	9.0	–	≤0.04	–
Mn	1.81	–	2.34	–	0.0007	–
Mo	0.39	–	≤0.2	–	≤0.0003	–
Ni	7.86	–	6.80	–	≤0.009	–
Ti	≤0.23	–	≤0.23	–	97.4	–
Zn	≤0.7	–	36.4	–	≤0.002	–

Table 2. Culture media

Compound	/mg L^{-1}	Compound	/mg L^{-1}
$CaCl_2 \cdot H_2O$	264.87	L-Methionine	15.00
KCl	400.00	L-Phenylalanine	32.00
$MgSO_4 \cdot 7H_2O$	200.00	L-Proline	11.50
NaCl	6800.00	L-Serine	10.50
$NaHCO_3$	2200.00	L-Treonine	48.00
$NaH_2PO_4 \cdot H_2O$	140.00	L-Trytophan	10.00
L-Alanine	8.90	L-Tyrosine	52.10
L-Arginine hydrochloride	126.00	L-Valine	46.00
L-Asparagine	15.00	Calcium pantothenate	1.00
L-Aspartic acid	13.30	Choline chloride	1.00
L-Cysteine	31.29	Folic acid	1.00
Glutamic acid	14.70	Inositol	2.00
L-Glutamine	292.00	Nicotinamide	1.00
Glycine	7.50	Pyridoxal hydrochloride	1.00
L-Histidine hydrochloride	42.00	Riboflavin	0.10
L-Isoleucine	52.00	Thiamine hydrochloride	1.00
L-Leucine	52.00	Glucose	1000.00
L-Lysine hydrochloride	72.00	Phenol Red	10.00

saturated calomel electrode (SCE) as reference electrode, and cold resin-mounted studs as working electrode with 1 cm^2 surface area. Polarization tests were performed at a 0.16×10^{-3} V s^{-1} scan rate.

The specimens were immersed in the CM electrolyte for up to 10 days and the EIS test was carried out as a function of time. Polarization tests were carried out on the GSS and GCZ studs after removing their gold coatings using mercury. The coating was removed to avoid pitting corrosion at the defects in the coating, and to allow comparison of the corrosion results of the three different substrates. The specimens were polarized from the E_{corr} to +1.3 V vs SCE after six days of immersion in the CM electrolyte.

Twelve pairs of studs were immersed in the CM electrolyte for 10 days. After this time the studs were removed and the CM electrolyte was analysed by the NAA method. 500 μL of each solution was pipetted and dried in a clean polyethylene capsule for irradiation

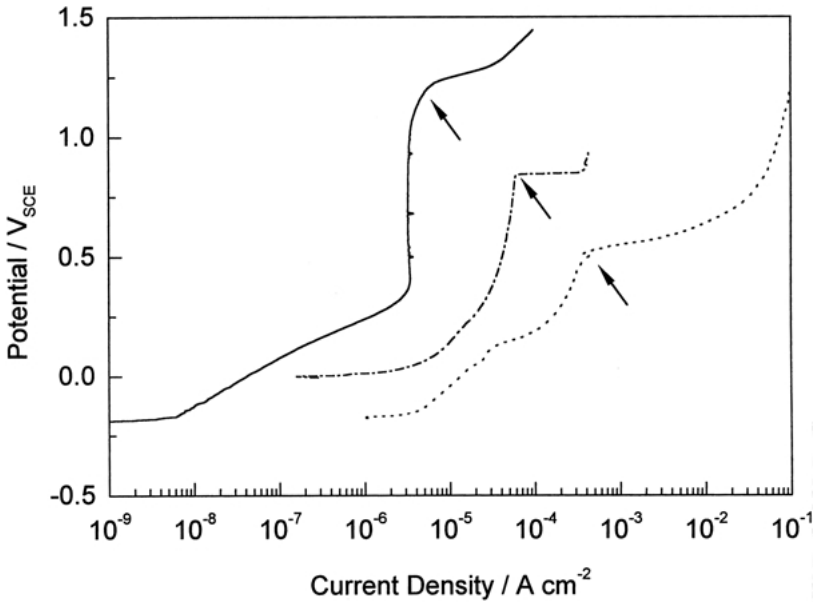

Fig. 1. Polarization curves for titanium and uncoated stud substrates after 6 days of immersion in a culture medium. (—) Titanium, (-•-) uncoated stainless steel, and (···) uncoated copper–zinc.

using an IEA-R1 nuclear reactor. The gamma ray spectra obtained were processed using the appropriate software and the concentrations of the elements calculated using a comparative method [8]. The blank of the CM electrolyte was also analysed in order to evaluate the contribution of its elements in the analysis of corrosion products.

Cytotoxicity assays were performed according to Rogero et al. and the ISO 10993 Standard [10,11], by adding diluted CM in which the studs remained immersed in Chinese hamster ovary cells culture (ATCC CHO k1). According to ISO 10993 Standard, cytotoxicity was determined quantitatively based on cell viability.

Finally, the stud surfaces were analysed using scanning electron microscopy (SEM) and energy dispersive X-ray (EDX) methods, before and after immersion in the CM electrolyte for 10 days. The studs were examined for coating defects which could expose the substrate and for reaction products on their surface.

3. Results and discussion

Figure 1 shows representative anodic polarization curves for uncoated stainless steel, uncoated copper–zinc alloy and titanium specimens after six days of immersion. The uncoated copper–zinc alloy presents the highest current density and the most active pitting potential (~0.5 V vs SCE), see arrows in Figure 1. A low current density is observed for the uncoated stainless steel substrate, up to high overpotentials, and a slight increase can be seen at ~0.85 V vs SCE. The titanium specimen showed the typical behaviour of an active corrosion reaction at low polarization (Tafel behaviour) in a large overpotential ~0.55 V vs SCE range. However, the low current density ($\sim 2 \times 10^{-6}$ A cm^{-2}) up to the oxygen evolution reaction potential indicates a passive titanium surface.

Figures 2 and 3 show typical Nyquist and Bode plots for GSS specimens after 1, 3, 6 and 10 days of

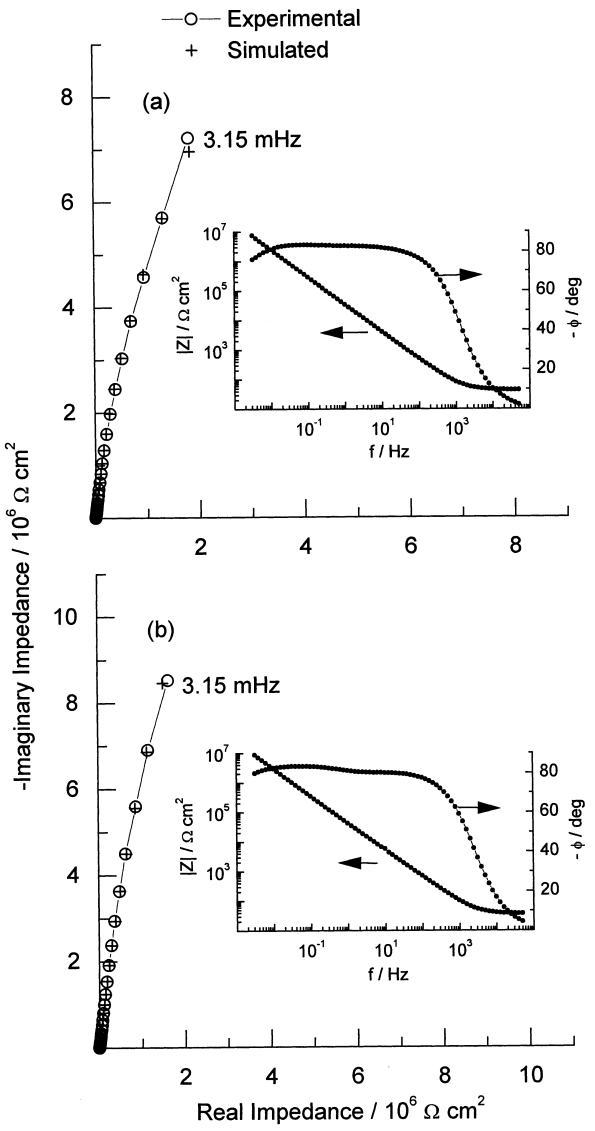

Fig. 2. Nyquist and Bode plots for gold-coated stainless steel (GSS) studs after 1 and 3 days of immersion in a culture medium.

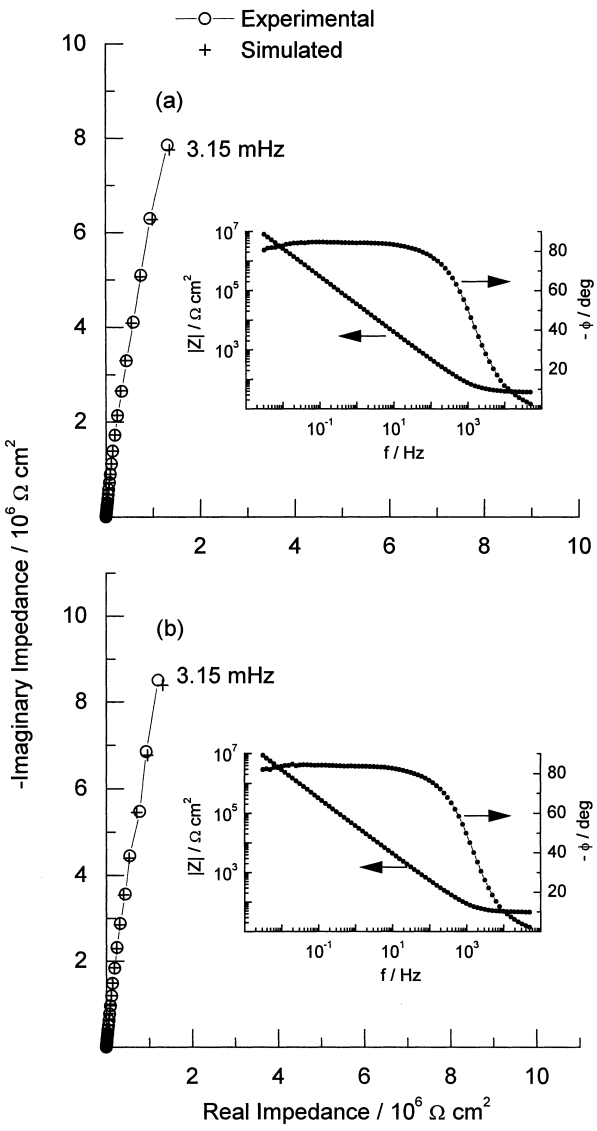

Fig. 3. Nyquist and Bode plots for gold-coated stainless steel (GSS) studs after 6 and 10 days of immersion in a culture medium.

Table 3. Parameters used in the simulation of impedance data for gold-coated stainless steel (GSS)/culture medium system*

Time /day	R_s /Ω cm^2	Y_{P1} /μF cm^{-2} s$^{-(1-\alpha1)}$	α_1	R_1 /Ω cm^2	Y_{P2} /μF cm^{-2} s$^{-(1-\alpha2)}$	α_2	R_2 /MΩ cm^2
1	43	101.44	0.72	10427	5.48	0.94	43
3	36	53.33	0.76	3741	4.46	0.93	121
6	36	544.09	0.57	9386	5.12	0.95	91
10	45	56.15	0.75	–	5.19	0.96	104

* For symbols, see text and Figure 4(a).

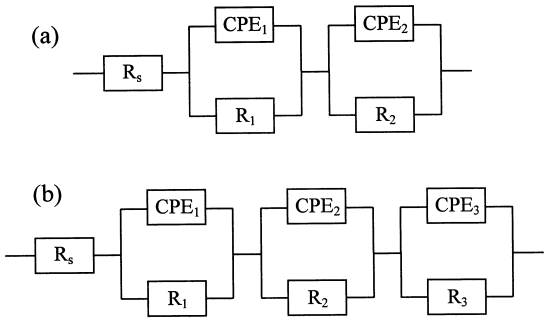

Fig. 4. Equivalent circuits used to model the ear piercing stud/culture medium system. R_S is the electrolyte resistance, R_1, R_2 and R_3 simulate processes taking place on the stud surface. The constant phase element (CPE) is $Y_{CPE} = Y_P(j\omega)^{\alpha}$, see text.

immersion in a CM electrolyte. A complex nonlinear least squares (NLLS) analysis was performed to fit the parameters of the equivalent circuit of Figure 4(a) to the impedance data. Fitted parameters are listed in Table 3. As can be observed in Figures 2 and 3, there is excellent agreement between the experimental and simulated results. Thus, Figure 4(a) is a good approach for modelling the GSS/CM electrolyte system. The Nyquist plots show a capacitive behaviour close to the 'ideal' indicated by large diameter depressed semicircles, suggesting that the gold coating covering the stainless steel studs has good protective properties. Unfortunately, the two capacitive loops, which according to the fitting procedure must exist (Table 3), are overlapped in the Nyquist plots of Figures 2 and 3 and cannot be observed. For this reason the inset Bode plots were included, showing two relaxation time constants, characterized by two maxima in the ϕ axis, defined at 10^{-2}–10^{-1} Hz and 10^{1}–10^{2} Hz. The capacitive behaviour corroborates the high corrosion resistance determined using the d.c. polarization method. Slight changes in the EIS response are observed up to 10 days of experimentation, lending further evidence of the good quality of the gold coating.

Figures 5 and 6 show representative Nyquist and Bode plots for GCZ studs after 1, 3, 6 and 10 days of immersion in a CM electrolyte. A NLLS analysis was performed to fit the parameters of the equivalent circuit of Figure 4(b) to the impedance data. Fitted parameters are listed in Table 4. There is excellent agreement between the experimental and simulated results. The Nyquist plots show three depressed capacitive semicircles (see the inset Bode plots, showing three time constants, characterized by three maxima in the ϕ axis). The two semicircles defined at high frequency are poorly separated. A more or less well defined depressed semicircle can be observed at low frequencies. Depressed semicircles indicate the interaction of several time constants, due to heterogeneity in the coating such as defects and an uneven surface. The high frequency relaxation process is related to some organic compound

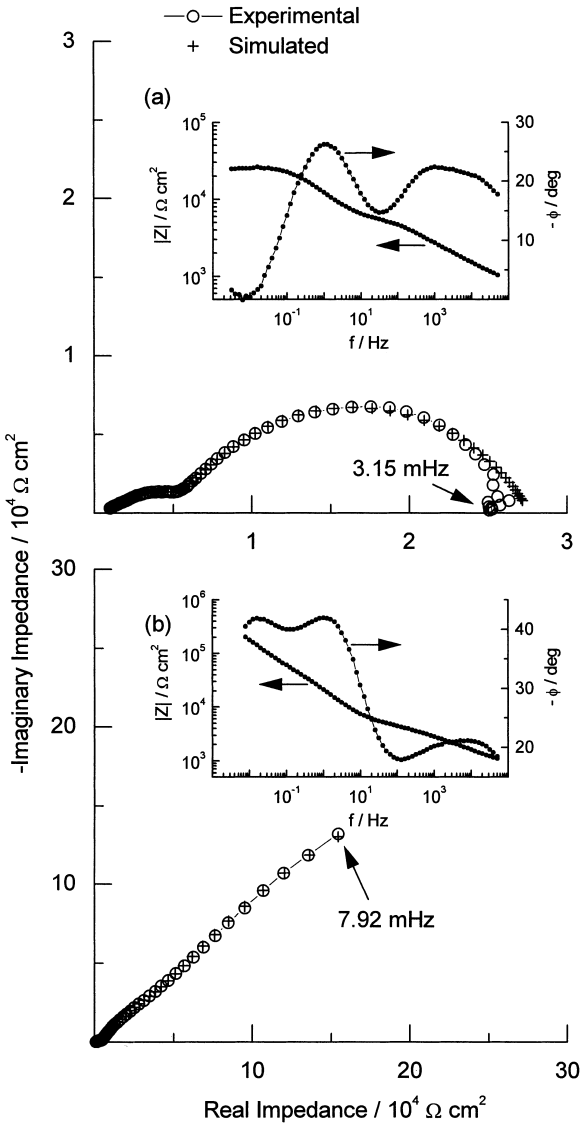

Fig. 5. Nyquist and Bode plots for gold-coated copper–zinc alloy (GCZ) studs after 1 and 3 days of immersion in a culture medium.

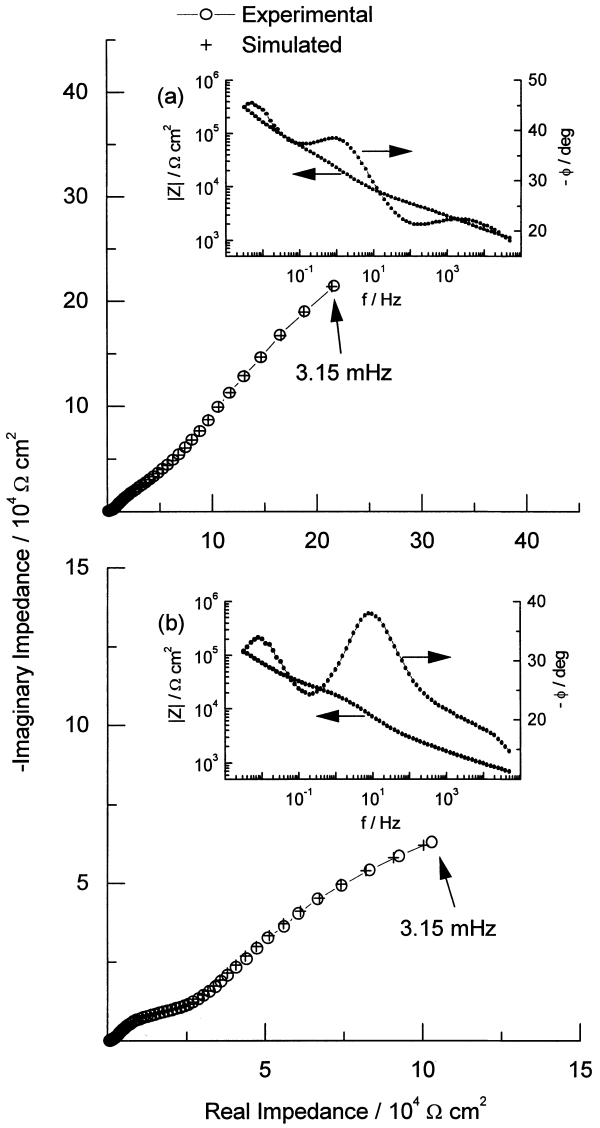

Fig. 6. Nyquist and Bode plots for gold copper–zinc alloy (GCZ) studs after 6 and 10 days of immersion in a culture medium.

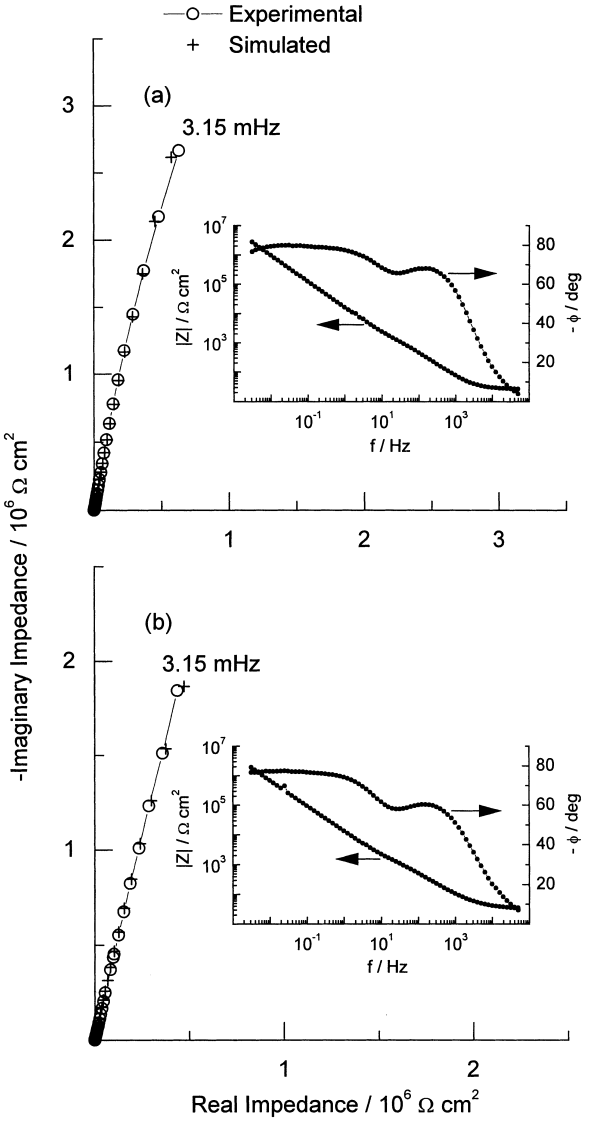

Fig. 7. Nyquist and Bode plots for titanium (Ti) studs after 1 and 3 days of immersion in a culture medium.

present in the CM electrolyte adsorbed on the electrode surface; the relaxation process at intermediate frequencies is related to the corrosion products precipitated in the defects and/or pores of the coating; finally, the relaxation process at low frequencies is related to the corrosion process at the base of the defects and/or pores of the coating, allowing the CM electrolyte to reach the metallic substrate. Significant changes take place in the Nyquist plots as the immersion time increased, both in the high and low frequency ranges. These changes may indicate that the GCZ studs were continuously corroding throughout the test period, even after corrosion products had been deposited in the defects, which seem to control the corrosion process.

Figures 7 and 8 show typical Nyquist and Bode plots for Ti specimens after 1, 3, 6 and 10 days of immersion

Table 4. Parameters used in the simulation of impedance data for gold-coated copper–zinc alloy (GCZ)/culture medium system*

Time/ day	R_s /Ω cm^2	Y_{P1} /μF cm^{-2} s$^{-(1-\alpha 1)}$	α_1	R_1 /Ω cm^2	Y_{P2} /μF cm^{-2} s$^{-(1-\alpha 2)}$	α_2	R_2 /Ω cm^2	Y_{P3} /μF cm^{-2} s$^{-(1-\alpha 3)}$	α_3	R_3 /Ω cm^2
1	535	6.89	0.43	4093	1.69	0.87	1147	29.03	0.69	21851
3	583	5.12	0.45	4530	21.54	0.75	24134	33.26	0.66	666330
6	571	7.70	0.42	5274	19.50	0.61	52891	54.27	0.71	1272700
10	437	12.54	0.43	2086	11.15	0.67	21182	90.58	0.63	265720

* For symbols, see text and Figure 4(b).

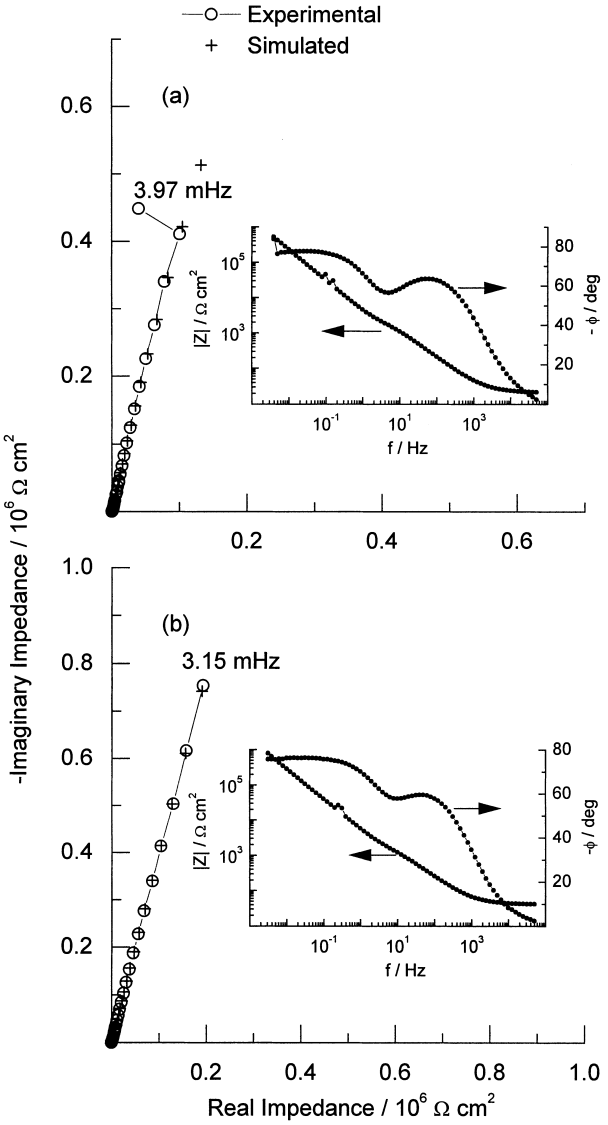

Fig. 8. Nyquist and Bode plots for titanium (Ti) studs after 6 and 10 days of immersion in a culture medium.

in a CM electrolyte. The behaviour of Ti specimens is similar to GSS specimens (Figures 2 and 3). A NLLS analysis was also performed to fit the parameters of the equivalent circuit of Figure 4(a) to the impedance data. Fitted parameters are listed in Table 5. As in the previous impedance data, there is excellent agreement between the experimental and simulated results. As in Figures 2 and 3 for the GSS/CM system, the Nyquist plots show two capacitive loops which are poorly separated in the frequency domain.

The equivalent circuit of Figure 4(a) contains two distributed constant phase elements (CPE_1 and CPE_2) to consider the two relaxation time constants (Figures 2, 3, 7 and 8). The CPE_1–R_1 couple, which predominates at high frequencies, may be originated by the passive film, while the CPE_2–R_2 couple, controlling at low frequencies, characterizes the properties of the film–solution interface. Similar results have been reported in the literature [12].

The admittance representation of the CPE (Y_{CPE}) shows a fractional-power dependent on the angular frequency (ω)

$$Y_{CPE} = Y_P(j\omega)^{\alpha} \tag{1}$$

where Y_P is a real constant and $-1 < \alpha < 1$. When $\alpha = 0$, CPE is a resistor; when $\alpha = 1$, a capacitor; and when $\alpha = -1$, an inductor. Finally, if $\alpha = 0.5$, CPE is the Warburg admittance.

As can be seen from Table 3, α_2 values are close to unity, indicating that CPE_2 is a capacitor and therefore Y_{P2} values may be directly assumed as capacitance values. The film thickness (L), in Å, may be calculated using the parallel plate condenser expression for the capacitance (C) in $\mu F\ cm^{-2}$ [13],

$$L = \frac{\varepsilon\rho}{0.113\,C} \tag{2}$$

where ε is the dielectric constant with a value of the order of 8.5 [14], and ρ is the surface roughness factor, the 1.2 value was used, which was reported for an iron surface mechanically polished using 600 grit emery [13]. By considering an intermediate value of $Y_{P2} = 5\ \mu F\ cm^{-2}$ (Table 3), a film thickness of $L = 18$ Å was obtained.

The α_2 values from Table 5 are of the order of 0.87, indicating that CPE_2 has an intermediate character between a capacitor ($\alpha_2 = 1$) and a Warburg impedance ($\alpha_2 = 0.5$). In this case, the oxide film suffers a deviation from the ideal capacitive behaviour. This deviation has been attributed in the literature to rough and uneven surfaces [15]. The α_2 values (Table 5) may indicate that the oxide film formed on titanium specimens in a CM electrolyte is inhomogeneous. It may be a consequence of an oxidation intermediate phase, probably leading to local defects, flaws and even oxide roughness if the corresponding oxidized species dissolve into the electrolyte [16].

Table 5. Parameters used in the simulation of impedance data for titanium/culture medium system*

Time /day	R_s /Ω cm²	Y_{P1} /μF cm^{-2} s$^{-(1-\alpha1)}$	α_1	R_1 /Ω cm²	Y_{P2} /μF cm^{-2} s$^{-(1-\alpha2)}$	α_2	R_2 /MΩ cm²
1	26	22.83	0.83	624	12.01	0.89	68
3	33	26.54	0.74	914	15.58	0.87	43
6	22	52.88	0.76	1078	46.72	0.87	11
10	41	56.77	0.75	652	36.19	0.85	55

* For symbols, see Figure 4(a).

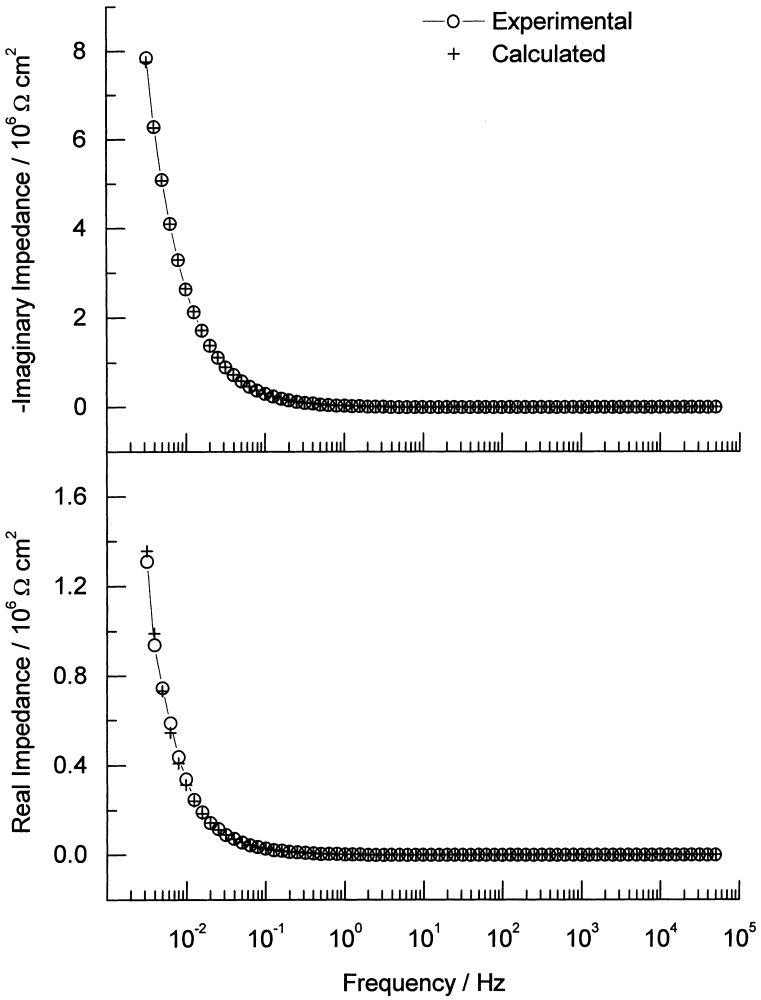

Fig. 9. Comparison of experimental data (○) and values calculated using K–K relations (+) for the GSS/CM system for 6 days.

As Y_{P2} from Table 5 cannot be assumed as a capacitance value (α_2 is not close to unity), the film thickness cannot be calculated. However, a fractal dimension of the oxide film may be estimated. The fractional exponent α_2 is directly related to the fractal dimension (D_f) [17], as

$$\alpha_2 = 1/(D_f - 1) \tag{3}$$

By considering an intermediate value of $\alpha_2 = 0.87$, a value of $D_f = 2.15$ was obtained.

On the other hand, R_2 values of the order of (50–80) $\times 10^6\ \Omega\ cm^2$ (Tables 3 and 5) indicate the low corrosion of the passive film corroborating a protective oxide.

Kramers–Kronig (K–K) relationships were applied to check the validity of experimental impedance results. K–K relationships can be used to determine the real part (or the imaginary part) of the transfer function of a causal, stable, linear, time invariant and finite system for $\omega \to 0$ and $\omega \to \infty$, when the change in the imaginary part (or the real part) with the angular frequency is known [18]. The imaginary part of the impedance

$$Z(\omega) = Z'(\omega) + jZ''(\omega) \tag{4}$$

is obtained, for example, using the real part values as follows

$$Z''(\omega) = -\frac{2\omega}{\pi}\int_0^\infty \frac{Z'(x) - Z'(\omega)}{x^2 - \omega^2}\,dx \tag{5}$$

where $Z'(\omega)$ and $Z''(\omega)$ are the real and imaginary parts of the impedance, respectively; x (integration variable) and ω angular frequencies (rad s^{-1}). Using Equation 5 it is possible to transform the real part into the imaginary part and vice versa [19–21].

The comparison of experimental plots with the plots calculated by the above method is a validation test for impedance measurements. Figures 9, 10 and 11, for example, report the results obtained with the impedance plots corresponding to six days of experimentation from Figures 3(a), 6(a) and 8(a), respectively. Three diagrams were chosen presenting GSS/, GCZ/ and Ti/CM electrolyte systems. The plots obtained using the K–K relationship, Equation 5, are visually close to the experimental plots, and it is concluded that Figures 3(a), 6(a) and 8(a) satisfy K–K relationships, signifying stability during time measure acquisition and relaxation processes for the ear piercing stud/CM system [18].

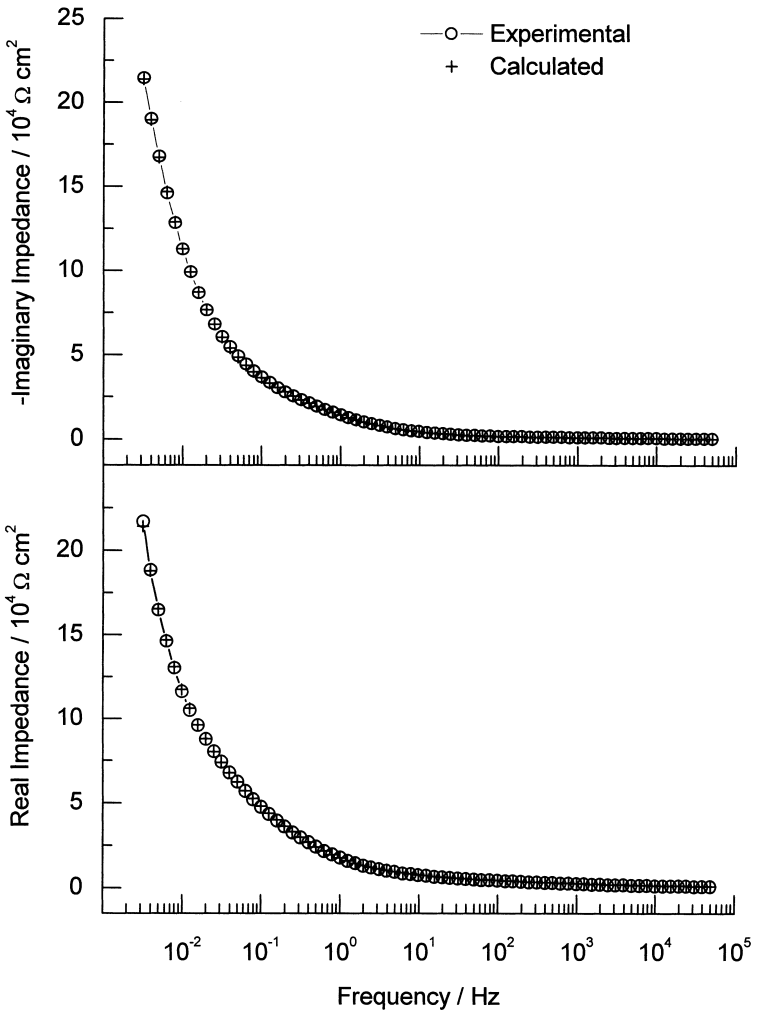

Fig. 10. Comparison of experimental data (○) and values calculated using K–K relations (+) for the GCZ/CM system for 6 days.

Figure 12 shows typical SEM results for a GCZ specimen. Defects were observed in the coating on GCZ studs before immersion in the CM electrolyte, see Figure 12(a). After a few days of immersion, corrosion products were seen on the GCZ stud surface, at regions with defects in the coating, see Figure 12(b). EDX analysis indicated that this product was zinc phosphate, see Figure 13. It should be noted that phosphate is a component of the CM electrolyte.

Table 6 shows chemical composition for the blank CM electrolyte and after immersion of the studs for 10 days of experimentation. Nickel was released from both gold-coated studs (GSS and GCZ specimens). This result indicates that despite the good corrosion resistance properties of the gold coating on stainless steel stud, nickel is released into the aggressive medium (CM electrolyte). Nickel released from substrate may lead to allergic reactions. The CM electrolyte in which stem substrates of GCZ studs were immersed presented a high zinc concentration, while the electrolyte with the GSS studs showed a high iron content. The high zinc content (six times higher than the blank) in the CM solution after 10 days of immersion of studs indicates that this element was leached from the substrate alloy, due to significant corrosion as corroborated by the EIS results. In the CM solution in which Ti studs were immersed, the elements detected were of the same order of magnitude as in the blank, indicating passivation of the Ti surface in the CM electrolyte.

The cytotoxic potential can be quantitatively expressed as a cytotoxicity index ($CI_{50\%}$), which is the concentration of the extract necessary to suppress colony formation to 50% of the control value. GSS and GCZ commercial studs showed cytotoxicity, presenting $CI_{50\%}$ of 78 and 44, respectively, and the latter (GCZ), higher toxicity. On the other hand, Ti studs were not cytotoxic, and the $CI_{50\%}$ was higher than 100.

4. Conclusions

The GSS and titanium studs presented the highest corrosion resistance. This fact may be partially attributed to the good quality of the gold coating on the GSS stud and partially to the high corrosion resistance of the stainless steel substrate and the uncoated titanium. Nevertheless, nickel was leached from the GSS stud substrates into the culture medium, presenting a cyto-

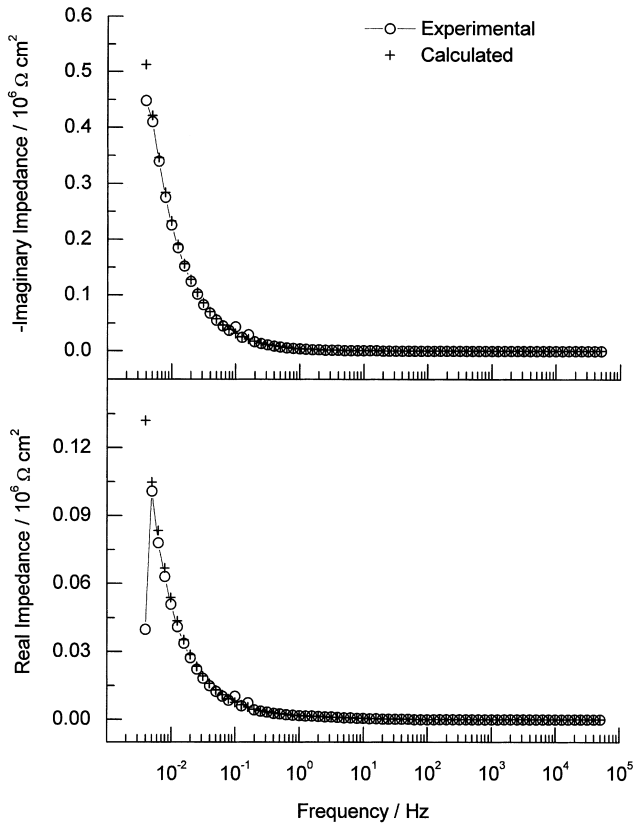

Fig. 11. Comparison of experimental data (○) and values calculated using K–K relations (+) for Ti/CM system for 6 days.

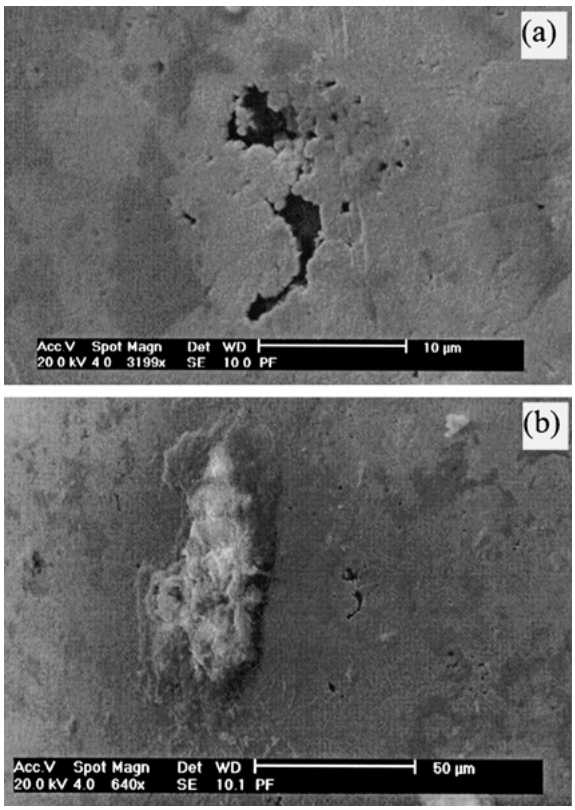

Fig. 12. (a) Precorrosion coating defects on a gold coated copper–zinc (GCZ) specimen. (b) Corrosion products on a corroded area of specimen (a).

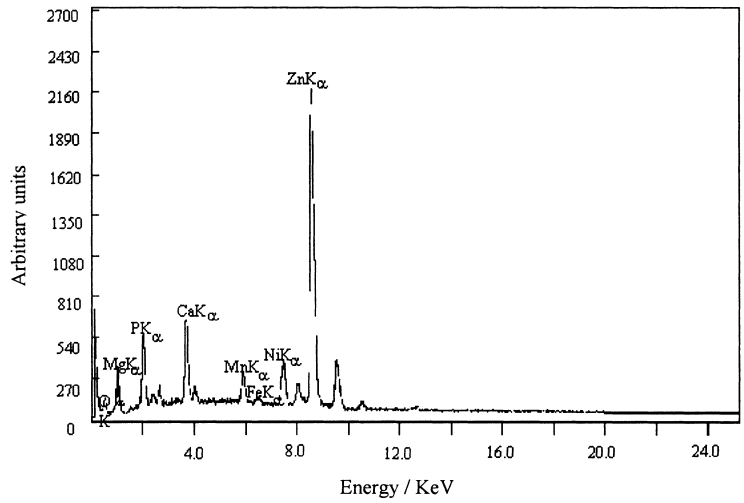

Fig. 13. EDX spectrum of the corroded area of Figure 12(b).

toxic effect. On the other hand, the GCZ studs provided the lowest corrosion resistance, releasing a significant amount of nickel due to their corrosion, and also showed cytotoxicity. The titanium stud offered the best combination of properties, with its high corrosion resistance, absence of nickel in its composition, and lack of cytotoxicity. These results underline the importance of using nickel-free materials for the manufacturing of ear piercing studs.

The shape of the Nyquist plots indicates a capacitive behaviour for the three types of studs tested, with a depressed capacitive loop at high frequencies originated by the film–solution interface, and a second capacitive loop at low frequencies characterizing the properties of the passive film on GSS and Ti studs. Three processes can observed in GCZ studs: a depressed capacitive loop at high frequencies characterizing the coating, a second capacitive loop at intermediate frequencies attributed to precipitation of corrosion products in the defects and/or pores of the coating, and a third capacitive response at low frequencies associated to the corrosion process inside pits. The applicability of Kramers–Kronig trans-

Table 6. Element concentration in the culture medium after 10 days

Element	Culture medium concentration/μg mL^{-1}			
	Blank	GSS	GCZ	Ti
Co	0.0121 ± 0.0012	0.099 ± 0.010	0.0616 ± 0.0005	0.0538 ± 0.0021
Cr	0.72 ± 0.02	0.73 ± 0.03	0.73 ± 0.04	0.75 ± 0.03
Fe	0.60 ± 0.09	4.03 ± 0.03	0.61 ± 0.08	0.43 ± 0.11
Ni	ND	0.66 ± 0.06	0.96 ± 0.09	ND
Zn	0.58 ± 0.05	0.61 ± 0.01	3.84 ± 0.41	0.75 ± 0.10

ND: Not detected.

forms for validating impedance data for the ear piercing stud/culture medium system has been assessed and the experimental impedance data has been found to satisfy K–K relations.

Acknowledgement

The authors express their gratitude to the FAPESP, Brazil, for financial support.

References

1. J.C. Wataha, R.G. Craig and C.T. Hanks, *J. Dent. Res.* **70** (1991) 1014.
2. R. Breitstadt, *Galvanotechnik* **83** (1992) 1691.
3. J. Rynänen, E. Niemi, W. Serlo, E. Niemela, P. Sandivik, H. Pernu and T.J. Salo, *J. Biomed. Mater. Res.* **35** (1997) 451.
4. Y. Ikarashi, J. Momma, T. Tsuchiya and A. Nakamura, *Biomaterials* **17** (1996) 2103.
5. J. Yang and K. Merrit, *J. Biomed. Mater. Res.* **28** (1994) 1249.
6. K. Bordji, J.Y. Jouzeau, D. Mainard, E. Payan, J.P. Delagoutte and P. Netter, *Biomaterials* **17** (1996) 491.
7. C. Meijer, M. Bredberg, T. Fischer and L. Vidströ, *Contact Dermatitis* **32** (1995) 147.
8. M. Saiki, S.O. Rogero, I. Costa, O.V. Correa and O.Z. Higa, *Radiat. Phys. Chem.* **55** (1999) 753.
9. L. Currie, *Anal. Chem.* **40** (1968) 586.
10. S.O. Rogero, F.J.C. Braga and O.Z. Higa, *Mater. Sci. Forum* **299/300** (1999) 44.
11. ISO 10993 Standard: Biological Evaluation of Medical Devices. Part 5. 'Tests for Cytotoxicity: *In Vitro* Methods'.
12. K. Azumi, T. Ohtsuka and N. Sato, *J. Electrochem. Soc.* **134** (1987) 1352.
13. M.E. Curley-Fiorino and G.M. Schmid, *Corros. Sci.* **20** (1980) 313.
14. D.D. Macdonald, K.M. Ismail and E. Sikora, *J. Electrochem. Soc.* **145** (1998) 3141.
15. U. Rammelt and G. Reinhard, *Electrochim. Acta* **35** (1990) 1045.
16. P.L. Cabot, J.A. Garrido, E. Perez, A.H. Moreira, P.T.A. Sumodjo and W. Proud, *Electrochim. Acta* **40** (1995) 447.
17. L. Nyikos and T. Pajkossy, *Electrochim. Acta* **30** (1985) 1533.
18. J.M. Bastidas, J.L. Polo, C.L. Torres and E. Cano, *Corros. Sci.* **43** (2001) 269.
19. P. Agarwal, M.E. Orazem and L.H. García-Rubio, *J. Electrochem. Soc.* **139** (1992) 1917.
20. C. Gabrielli, M. Keddam and H. Takenouti, *in* J.R. Scully, D.C. Silverman and M.W. Kendig (Eds), 'Electrochemical Impedance: Analysis and Interpretation', ASTM STP 1188, Philadelphia (1993), pp. 140–153.
21. D.D. Macdonald and M. Urquidi-Macdonald, *J. Electrochem. Soc.* **132** (1085) 2316.